Flow Property at Capillary Extrusion for Ethylene-Tetrafluoroethylene Copolymer

Seigo Kotera,[1,2)] Masayuki Yamaguchi[1)*]

1) School of Materials Science, Japan Advanced Institute of Science and Technology,
1-1 Asahidai, Nomi, Ishikawa 923-1292 JAPAN

2) Asahi Glass Co., Ltd.,
1150 Hazawa-cho, Kanagawa-ku, Yokohama 221-0863 JAPAN

* Correspondence to:
Masayuki Yamaguchi
Phone +81-761-51-1621, Fax +81-761-51-1621
e-mail m_yama@jaist.ac.jp

Abstract

The capillary extrusion property of ethylene-tetrafluoroethylene copolymer (ETFE) is evaluated. It is found that ETFE shows several types of flow instabilities. The shark-skin failure is observed over the first critical shear stress 7.9×10^4 Pa. Then, the slip-stick instability is detected at 1.8×10^5 Pa, which corresponds to the critical stress of the slippage at the die wall, evaluated by the Mooney method. Moreover, gross wavy melt fracture appears at high out-put rate condition. It is interesting to note that quasi-stable flow region; so-called “super-extrusion” is observed between slip-stick and wavy melt fracture regions. Because of the steady slippage, ETFE can be extruded at a high out-put rate condition without surface roughness and distortion of extrudates.

Keywords:

Ethylene-tetrafluoroethylene copolymer; Rheological properties; Extrusion; Melt fracture

1. Introduction

It has been well known that flow instability at capillary extrusion is roughly classified into two categories; surface instability known as shark-skin failure and gross, volumetric, and wavy melt fracture [1-4]. Meller et al. summarized that the shark-skin failure occurs beyond the critical shear stress at the die exit and the wavy melt fracture takes place beyond the critical elongational stress at the die entry [5]. Therefore, the rheological properties, especially strain-hardening behavior in elongational viscosity, affect the type of flow instability. For example, linear low-density polyethylene (LLDPE) having no strain-hardening shows the shark-skin failure at low shear rate, whereas low-density polyethylene with long-chain branches (LDPE), that is known to show marked strain-hardening in elongational viscosity, exhibits the wavy melt fracture prior to shark-skin. Moreover, there are at least two origins of the shark-skin failure [2-4,6]; one is the cohesive rupture by the sudden deformation of the surface area after passing the die exit, and the other is the irregular slippage. The critical stresses of both mechanisms were discussed by Allal et al., which were summarized in the following relations [7,8],

$$\sigma_c = \frac{1}{2} G_N^0 \frac{N_e}{\sqrt{N_0}} \tag{1}$$

$$\sigma_s = \frac{9}{4\pi} G_N^0 C_{ad} \frac{N_e}{\sqrt{N_0}} \tag{2}$$

where $G_N{}^0$ is the rubbery plateau modulus, N_e is the number of monomers between entanglements and N_0 is that of monomers per chain, and C_{ad} is the factor expressing the fraction of a polymer absorbed on the wall surface.

Since the average molecular weight between entanglement couplings M_e is

inversely proportional to G_N^0, a polymer having high M_e tends to show shark-skin failure at low shear stress [9]. Furthermore, it has been clarified that the narrow distribution of molecular weight also leads to the flow instability at low shear stress, which was theoretically derived using the concept of Deborah number [9].

Besides the control of molecular weight distribution, the flow instability is avoided by the addition of various types of processing aids. It is well known that some fluoropolymers such as vinylidene fluoride and hexafluoropropylene copolymer are employed as the processing aid to minimize the shark-skin failure [3]. In particular, they are frequently used for LLDPE. The addition lowers the extrusion stress by steady slippage at the die wall and thus the shark-skin failure does not occur even at high out-put rate condition.

When a fluoropolymer itself is processed at extrusion, the flow instability should be also considered seriously, because it decides the production speed. However, there have been only a couple of reports on the flow instability of fluoropolymers. Hatzikiriakos et al. reported that typical perfluoropolymers such as poly(tetrafluoroethylene-*co*-perfluoroalkylvinylether) (PFA) and poly(tetrafluoroethylene-*co*-hexafluoropropylene) (FEP) show a relatively low critical onset shear stress of shark-skin failure by the capillary extrusion [3]. They also revealed that the addition of specific fillers, e.g., Boron nitride, can increase the critical shear stress, leading to high out-put rate operation. According to them, Boron nitride plays a role on the internal lubricant to stabilize the streamlines at the die entrance. Rosenbaoum, one of their colleagues, studied instable phenomena of FEP at capillary flow and summarized the types of flow instabilities [10]. According to him, “super-extrusion region” is observed between slip-stick and wavy melt fracture regions

in the case of FEP. The effect of fluorine content in fluoropolymers on the capillary extrusion properties was investigated by Chen et al., as compared with polyethylene and perfluorinated polymers [11]. They reported that perfluorinated polymers tend to exhibit the flow instability even at a low shear stress and a partially fluorinated polymer like ethylene-tetrafluorethylene (ETFE) copolymer shows different flow instability that depends on the fluorine content.

The poor information on the flow instability for fluoropolymers is a serious problem for the industrial application, because the demand of melt-processable fluoropolymers increases recently due to the excellent electrical properties, surface properties, and chemical and thermal stability. Among them, intense attention has been focused on ETFE, which is often used in the forms of sheet, film, and wires [12,13]. Therefore, it is important to comprehend the processability at extrusion including the flow instabilities. Since it is predicted that G_N^0 of ETFE is much lower than that of polyethylene, the shark-skin failure is expected to occur at a low shear stress and limits the out-put rate. Therefore, the understanding of the flow instability at capillary extrusion is inevitable for the industrial application of ETFE.

2. Experimental

2-1. Material

A commercially available terpolymer comprising of ethylene, tetrafluoroethylene, and 3,3,4,4,5,5,6,6,6-nonafluorohexene ($CH_2CHC_4F_9$; NFH), was employed in this study. The details of the characteristics were mentioned in our previous paper [14]. The melt flow rate is 11.8 [g/10 min] (297 °C, 49 N) and the melting point is 258.7 °C.

2-2. Measurements

Frequency dependence of the oscillatory shear modulus was measured by a cone-and-plate rheometer, (TA instrument, Ares GII) at 260 – 300 °C. The diameter of the plates is 25 mm. The preheating time before the measurement was 5 min. In order to clarify the thermal stability, the measurements were performed without changing the sample. The angular frequency decreases from 628 to 0.314 s^{-1}.

The steady-state shear viscosity was measured by a capillary rheometer (Toyoseikiseisakusyo, Capirograph 1C) at 300 °C using various types of circular dies shown in Table 1.

Table 1 Dies used in this research

Die	*D* (mm)	*L* (mm)	Entrance Angle (degree)
#1	1	40	180
#2	1	20	180
#3	1	10	180
#4	2	20	90
#5	0.8	8	90
#6	0.5	5	90

The shear rate and shear stress were calculated by the Hagen-Poiseuille law with the Bagley and Weissenberg-Rabinowitsch corrections. The complex shear viscosity was calculated from the oscillatory moduli. The angular frequency ω is converted to the shear rate $\dot{\gamma}$ by applying the following Cox-Merz rule.

$$\eta(\dot{\gamma}) = \eta^*(\omega)\Big|_{\omega\to\dot{\gamma}} \qquad (3)$$

$$\eta^*(\omega) = \frac{\sqrt{G'(\omega)^2 + G''(\omega)^2}}{\omega} \quad (4)$$

The appearance of the extruded strands was observed by an optical microscope to evaluate the flow instability.

3. Results and discussion

Figure 1 shows the master curves of angular frequency dependence of oscillatory shear modulus at 300 °C. The time-temperature superposition principle seems to be applicable in this temperature range, although thermal degradation occurs slightly at 300 °C [14]. The storage modulus *G'* and loss modulus *G"* are proportional to ω^2 and ω, respectively, in the low frequency region; i.e., the rheological terminal zone is observed.

The flow activation energy, calculated by the Andrade equation, is found to be 89 kJ/mol, which is slightly larger than the value reported previously, 65 kJ/mol [15]. These values are intermediate between the typical values of linear polyethylene (21-30 kJ/mol) and that of polytetrafluoroethylene (PTFE) (75-150 kJ/mol) [16-22]. The modulus of the crossover point, i.e., $G_x = G' = G''$, is 1.3×10^5 Pa and the angular frequency of this point is 1.1×10^3 s^{-1}. According to the empirical relation proposed by Wu [23], the rubbery plateau modulus G_N^0 is given by the following relation.

$$\log\left(\frac{G_N^0}{G_x}\right) = 0.380 + \frac{2.36\log\left(M_w/M_n\right)}{1 + 2.45\log\left(M_w/M_n\right)} \quad (5)$$

Since M_w/M_n of the present sample was found to be 2.0 [14], G_N^0 is calculated to be 1.2×10^5 Pa. The value is significantly lower than that of polyethylene, 2.3×10^6 Pa [24].

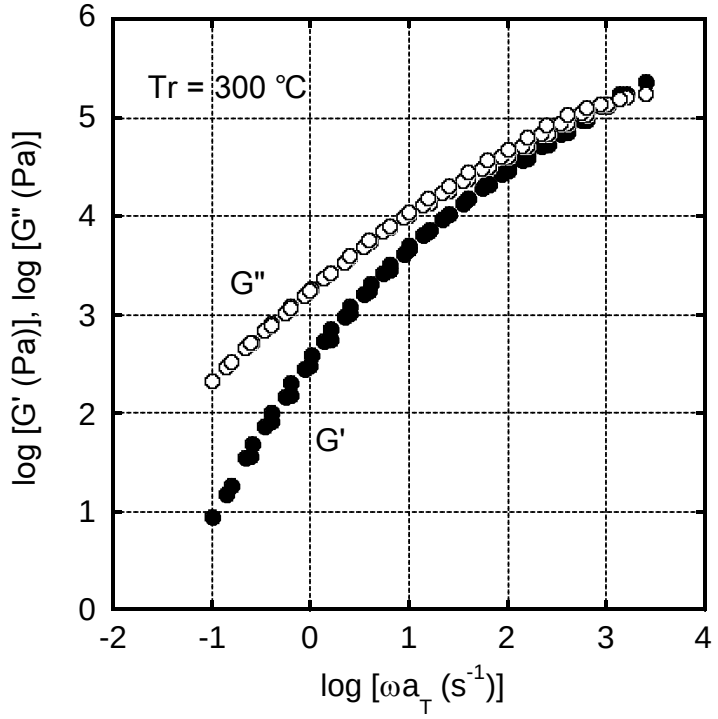

Figure 1 Master curves of the frequency dependence of the oscillatory shear moduli such as storage modulus *G'* and loss modulus *G"* at 300 °C.

Furthermore, the figure provides the rheological terminal parameters such as zero-shear viscosity η_0 and steady-state shear compliance J_e^0 as follows;

$$\eta_0 = \lim_{\omega \to 0} \frac{G''}{\omega} \tag{6}$$

$$J_e^0 = \lim_{\omega \to 0} \frac{G'}{\omega^2} \tag{7}$$

The value of η_0 is 1.8 × 10^3 Pa s at 300 °C. It has been known that J_e^0 is proportional to $(M_z/M_w)^{3.7}$ [25]. Furthermore, the value of a monodispersed polymer J_e^{00} has a relationship with G_N^0 as follows [24];

$$J_e^{00} = \frac{4}{G_N^0} \tag{8}$$

The molecular weight distribution of the present sample is expressed by the Shulz-Zimm distribution [26] and M_w/M_n was found to be 2.0 as mentioned. Therefore,

the value of M_z/M_w should be 1.5. Since J_e^0 is 1.45 × 10^{-4} Pa^{-1} from the figure, G_N^0 is calculated to be 1.2 × 10^5 Pa. The value corresponds with the result obtained from G_x.

Figure 2 shows the steady-state shear viscosity $\eta(\dot{\gamma})$ evaluated by the capillary rheometer using the dies #1-3 and the absolute value of the complex shear viscosity $|\eta^*(\omega)|$ at 300 °C. The Bagley and Weissenberg-Rabinowitsch corrections were applied to the evaluation of the flow curve.

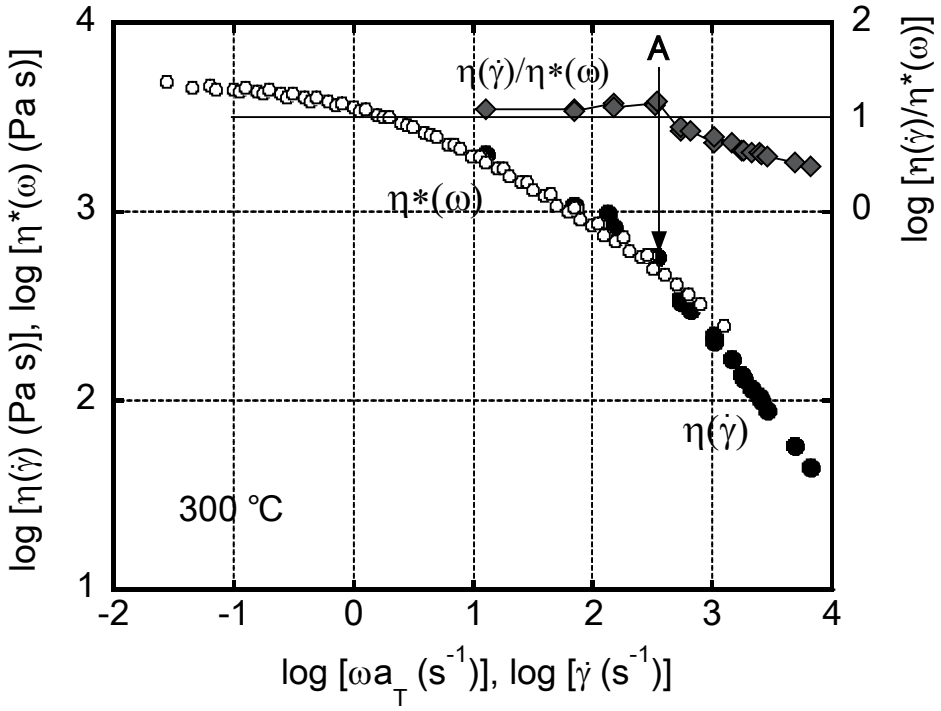

Figure 2 Flow curves at 300 °C. (closed circles) steady-state shear viscosity η as a function of shear rate $\dot{\gamma}$ and (open circles) complex viscosity η^* as a function of angular frequency ω. The ratio of η and η^* is also plotted.

The shear-thinning behavior is clearly detected in the wide range of shear rates. Moreover, the Cox-Merz rule is applicable in the low shear rate region. In contrast, it is clear that $\eta(\dot{\gamma})$ is lower than $|\eta^*(\omega)|$ in the high shear rate, i.e., beyond the point "A", which is defined by the value of η/η^* as shown in the figure.

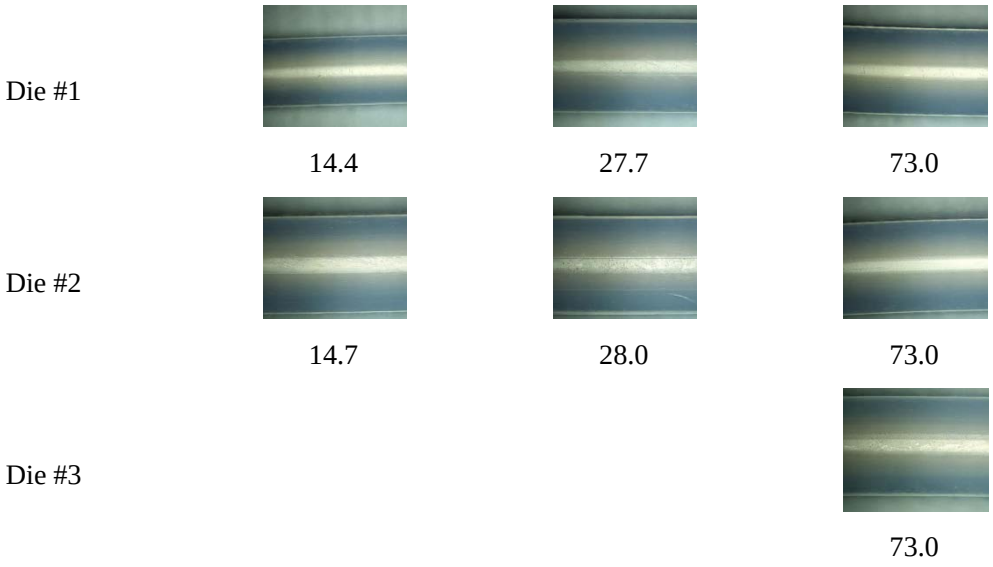

(a) Stable flow region 14.4 - 73.0 s^{-1}

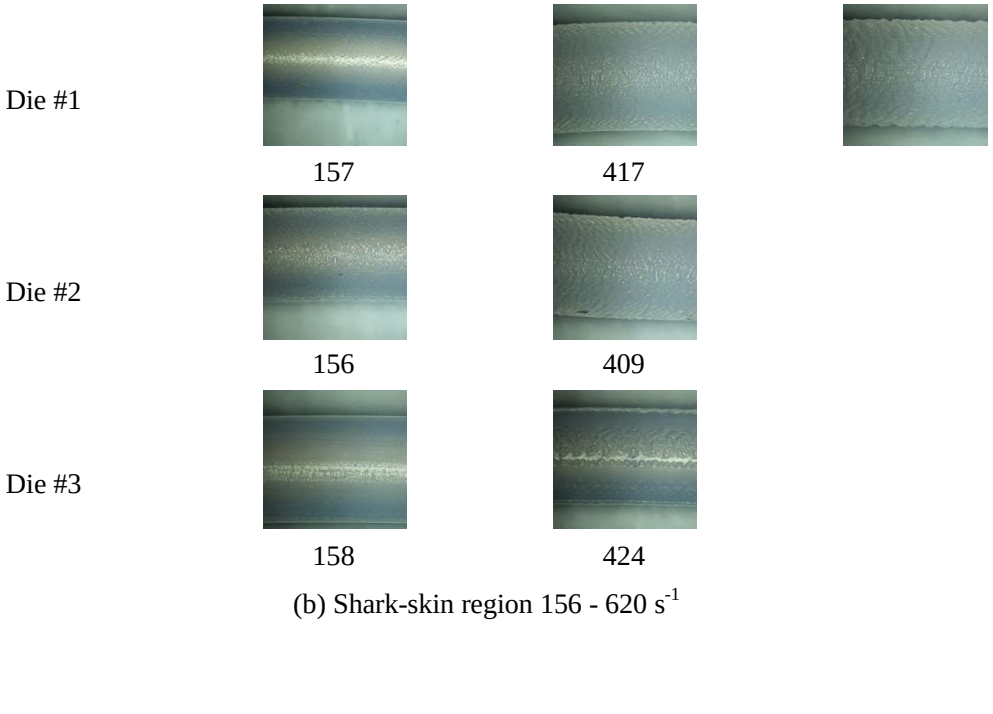

(b) Shark-skin region 156 - 620 s^{-1}

(c) Slip-Stick region around at 591 s^{-1}

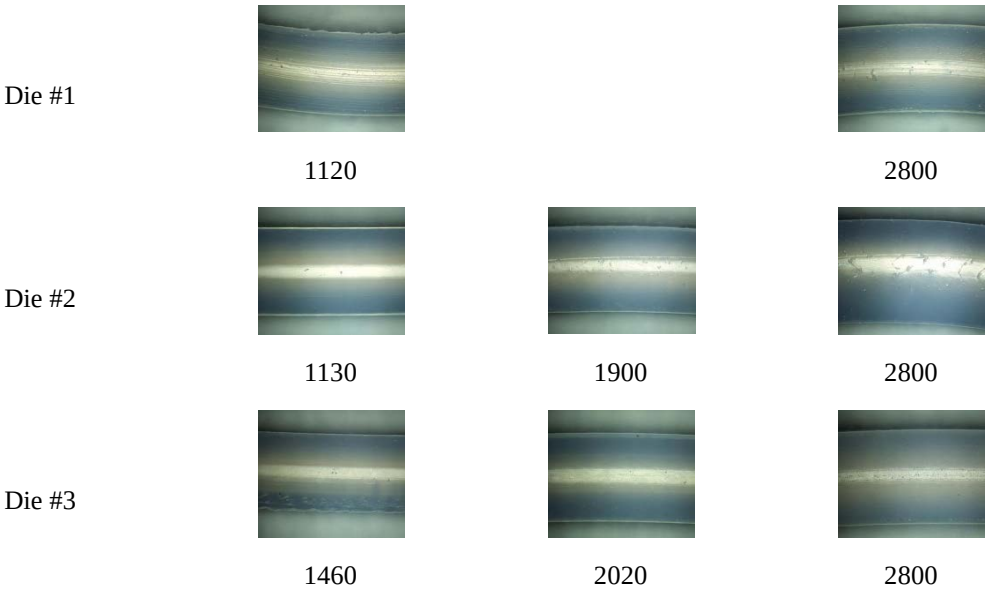

(d) Super-extrusion region 1120-2800 s^{-1}

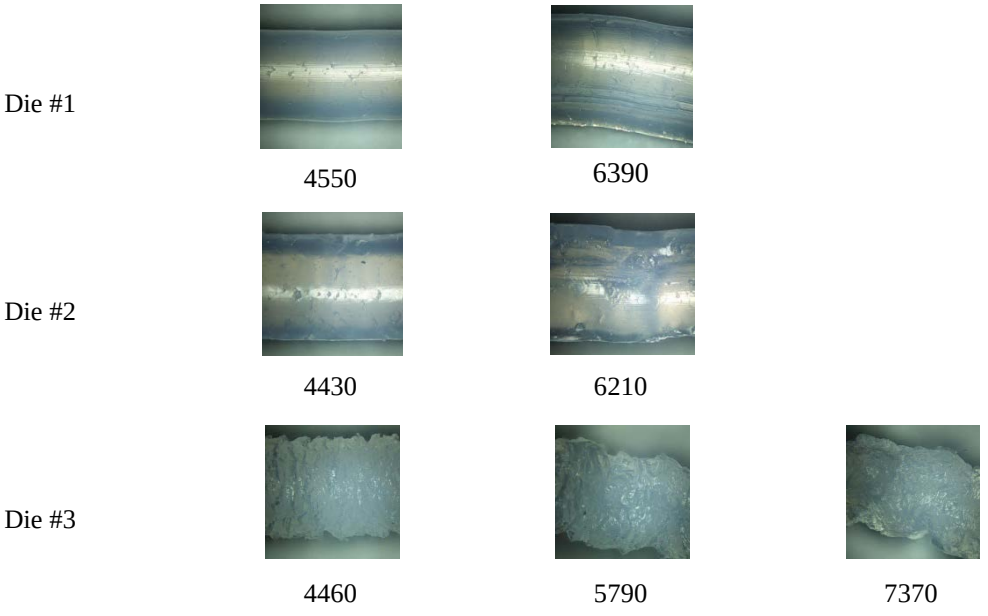

(e) Wavy melt fracture region 4430-7370 s^{-1}

Figure 3 Optical micrographs of the strands extruded at various shear rates at 300 °C; (a) stable flow region 14.4 – 73 s^{-1}, (b) shark-skin region 156 – 620 s^{-1}, (c) slip-stick region 591 s^{-1}, (d) super-extrusion region 1130 – 2800 s^{-1}, and (e) wavy melt fracture region 4430 – 7370 s^{-1}. The numerals represent the shear rates on the wall, which are corrected by the Weissenberg-Rabinowitsch method.

For the better understanding of this phenomenon, the extruded strands were observed by the optical microscope as shown in Figure 3. It is noted that ETFE shows three types of flow instabilities and a quasi-stable flow region with increasing the shear rate. At first, the strands with smooth surface are obtained in the lowest shear rate region, as shown in Figure 3(a). The maximum shear rate in this first stable region is 73 s^{-1} and the shark-skin instability is observed at 156 s^{-1}. It indicates that the critical shear stress for the shark-skin instability is between 7.9×10^4 Pa and 1.3×10^5 Pa. Although the value is slightly lower than those of polyethylene, $1 - 2 \times 10^5$ Pa [4], the difference between them is not so significant. It is interesting because ETFE has narrow molecular weight distribution, leading to low critical stress [9], as compared with commercialized polyethylene. Based on the difference in G_N^0, however, the critical stress of ETFE is predicted to be ten time as low as that of polyethylene from equations (1) and (2). Although the molecular weight of ETFE, i.e., N_0 in the equations, is unknown, the theory will not be applicable for the present polymer.

As shown in Figures 3(b) and (c), the shark-skin failure occurs in the shear rate up to 620 s^{-1}, irrespective of the die length. Then, the slip-stick failure is detected at 591 s^{-1} for the die #2. Moreover, it should be notified that the strand extruded in the shear rate region from 1120 to 2800 s^{-1} has smooth surface as shown in Figure 3(d), although the shear rate is much higher than those in the shark-skin and slip-stick regions. The phenomenon is known as “super-extrusion” that is previously reported for linear polymers, such as LLDPE, PTFE, FEP, polybutadiene, and others [20,27,28].

In the high shear rate region, e.g., 4430 s^{-1}, the wavy melt fracture (WMF) appears. As shown in Figure 3(e), WMF is reduced using the die with long length. This is reasonable because the flow instability at the die entry, which is the origin of WMF, is

healed to some degree in the die land.

The flow curve is shown in Figure 4 with the notification of flow instability and quasi-stable flow regions, in which the shear rate and shear stress are corrected by the Bagley and Weissenberg-Rabinowitsch corrections. The super-extrusion region is clearly observed in the wide range of shear rates.

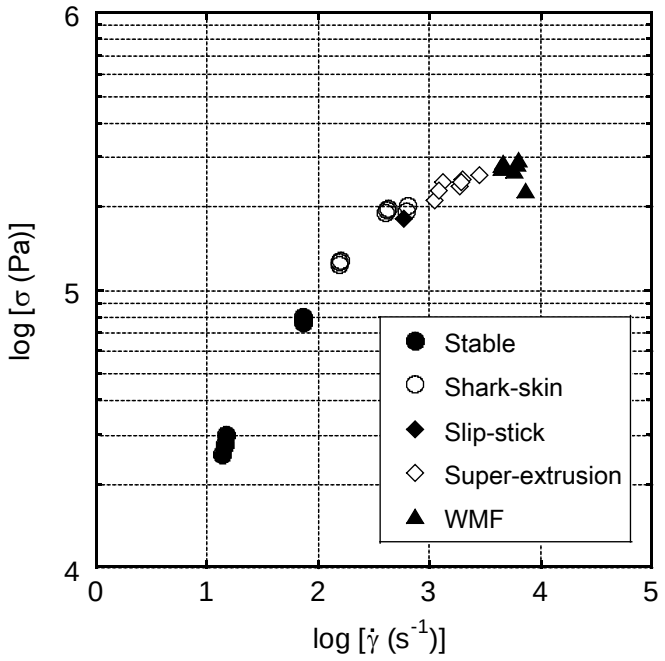

Figure 4 Flow curves at 300 °C with notification of flow behaviors; (closed circles) stable flow, (open circles) shark-skin, (closed diamonds) slip-stick, (open diamonds) super extrusion, and (closed triangles) wavy melt fracture.

Rosenbaoum reported the flow curve of FEP with the illustration of various flow instabilities [10]. Figure 5 compares the shear stress and flow instabilities for ETFE and FEP, in which the horizontal axis represents the apparent shear rate using the die #1 (L/D=40/1). It is found that ETFE shows a similar behavior to FEP; i.e., stable, shark-skin, super-extrusion, and WMF region. However, the slip-stick failure is not detected in the case of the die #1 for ETFE, whereas FEP exhibits the slip-stick in the

wide range of shear rates. Even when using the die #2, the slip-stick failure occurs only in the limited shear rate range for ETFE. The results suggest that the friction on the die wall is different between them and the slip-stick failure would occur in the limited shear rate range.

The slip velocity at the die wall can be evaluated by the Mooney analysis [3]. When the slip velocity at the die wall is decided by the apparent shear stress σ_a, the apparent shear rate $\dot{\gamma}_a$, given by equation (9), has the linear relationship with the inverse of the radius of dies, $1/R$. Then, the slip velocity V_{slip} is predicted using equation (11).

$$\dot{\gamma}_a = \frac{4Q}{\pi R^3} \tag{9}$$

$$\sigma_a = \frac{\Delta P}{L} \cdot \frac{R}{2} \tag{10}$$

$$\dot{\gamma}_a = 4V_{slip}\frac{1}{R} + \dot{\gamma}_{a,\,slip-corrected} \tag{11}$$

where Q is the volumetric flow rate, $\Delta P/L$ is the pressure gradient in the die, and $\dot{\gamma}_{a,\,slip-corrected}$ is the shear rate considering the slippage at the die wall without the Weissenberg-Rabinowitsch correction.

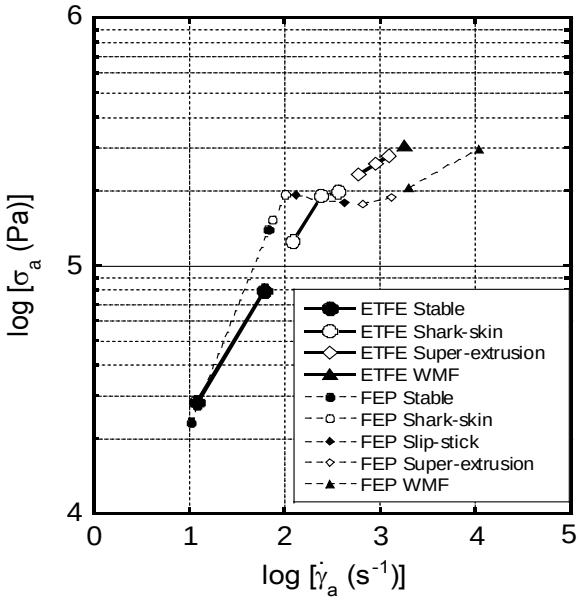

Figure 5 Comparison of flow behaviors for (bold lines) ETFE and (dotted lines) FEP [15]; (closed circles) stable flow, (open circles) shark-skin, (closed diamonds) slip-stick, (open diamonds) super-extrusion, and (closed triangles) wavy melt fracture. Both shear rate and shear stress represent the apparent values without the corrections.

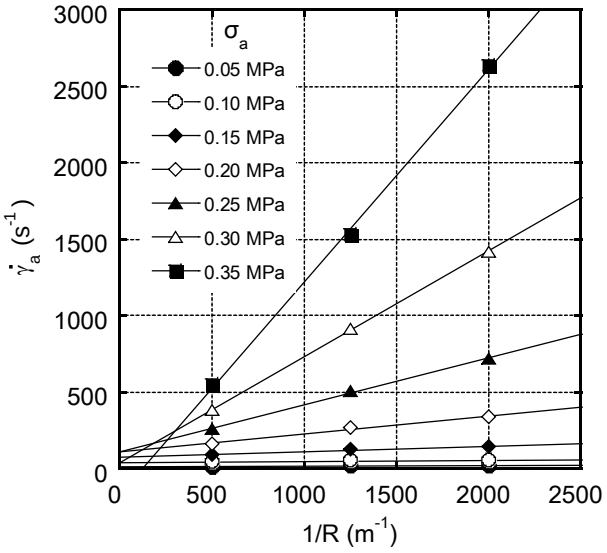

Figure 6 Mooney analysis at 300 °C using various dies #4-6; The stress levels are (closed circles) 0.05 MPa, (open circles) 0.10 MPa, (closed diamonds) 0.15 MPa, (open diamonds) 0.20 MPa, (closed triangles) 0.25 MPa, (open triangles) 0.30 MPa, and (closed squares) 0.35 MPa.

The capillary flow measurements were performed using various dies with the same L/D ratio (#4 to 6). Therefore, the difference in the pressure loss at the inlet and die exit among the dies is negligible.

The linear relations between apparent shear rate and $1/R$ are confirmed as shown in Figure 6, suggesting that the slip velocity is constant. When σ_a is lower than 3×10^5 Pa, the intercept values increase with increasing σ_a. Beyond 3.5×10^5 Pa, however, V_{slip} cannot be estimated properly. Furthermore, the super-extrusion region also appears at this experiment. Figure 7 exemplifies the extruded strand using the die #4. The super-extrusion region is clearly observed from 2.5×10^5 to 3.5×10^5 Pa (Figure 8), suggesting that the steady slippage occurs irrespective of the entrance angle of the die.

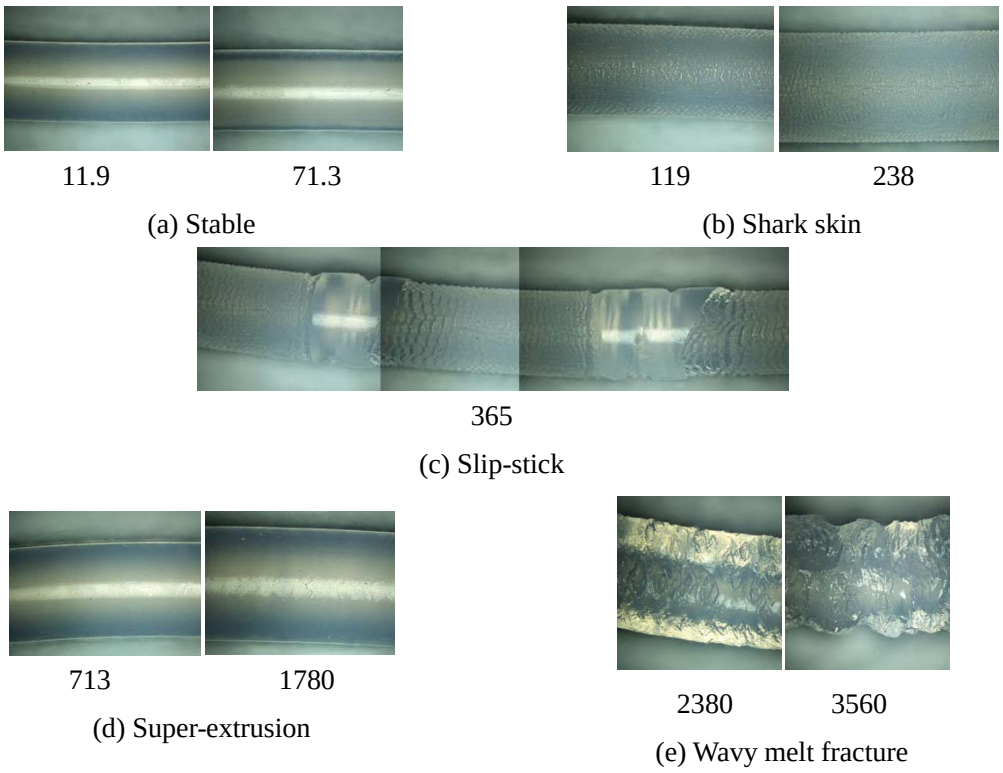

Figure 7 Optical micrographs of the strands extruded from die #5 at 300 °C; (a) stable flow region, (b) shark-skin region, (c) slip-stick region, (d) super-extrusion region, and (e) wavy melt fracture region. The numerals represent the apparent shear rate [s^{-1}] on the wall.

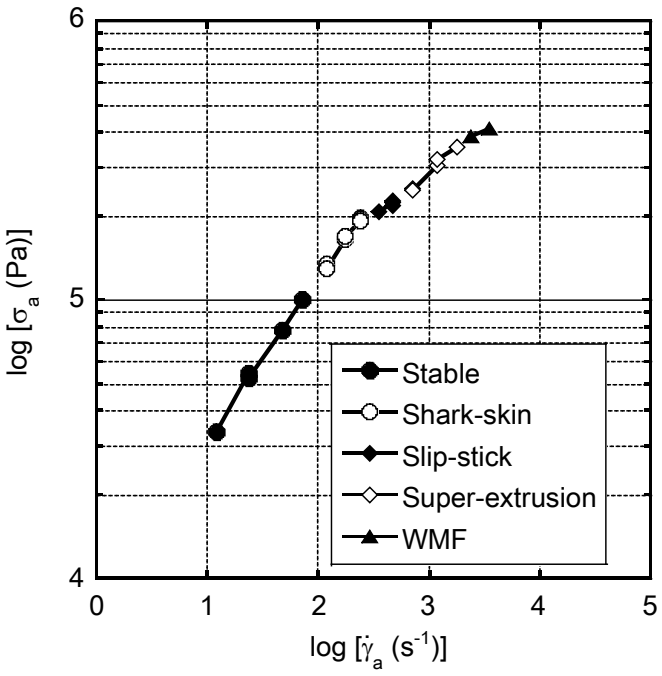

Figure 8 Flow curve obtained using die #4 at 300 °C; (closed circles) stable flow, (open circles) shark-skin, (closed diamonds) slip-stick, (open diamonds) super extrusion, and (closed triangles) wavy melt fracture. Both stress and shear rate are the apparent values.

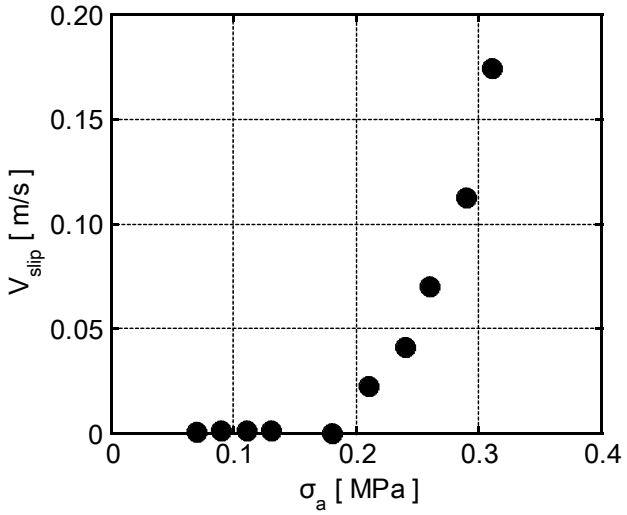

Figure 9 Slip velocity as a function of the apparent shear stress on the wall at 300 °C.

Finally, we made further analysis on the critical shear stress of the slippage to clarify the relationship between the wall slippage and flow instabilities. The slip velocity V_{slip} evaluated by the Mooney analysis is plotted against the apparent shear stress σ_a in Figure 9. Obviously, V_{slip} begins to increase beyond 1.8×10^5 Pa, which can be regarded as the critical shear stress of the slippage for ETFE at 300 °C. It should be noted that the stress at the boundary point from shark-skin to slip-stick is 1.8×10^5 Pa, indicating that the actual slippage at the wall triggers the change from shark-skin to slip-stick at capillary extrusion. Furthermore, the slippage is also responsible for the difference between η and η^* in Figure 2. In other word, due to the slippage, the steady-state shear viscosity η is lower than the complex shear viscosity η^* in the shear rate region beyond the point A.

As for the super-extrusion phenomenon, the detail mechanism has not been clarified yet. However, it is known that the velocity profile in the capillary is rather plug-type flow because of the significant slippage [28]. According to the previous researches [4], the following relationship was detected in the super-extrusion region,

$$V_{slip} = \alpha \sigma_a{}^m \qquad (12)$$

where α and m are the constants.

For the present sample, as shown in Figure 10, the power-law relationship is detected in the super-extrusion region. The upper limit of the shear stress would be decided by the onset of WMF. The lowest value is, on the other hand, determined by the critical stress of the “stick” on the die wall. Based on the theory proposed by Brochard and de Genne [6], the entanglement couplings between polymer chains adsorbed on the wall and polymer chains flowing near the die wall are responsible for the stick. When the applied stress is beyond the critical value, steady slippage occurs.

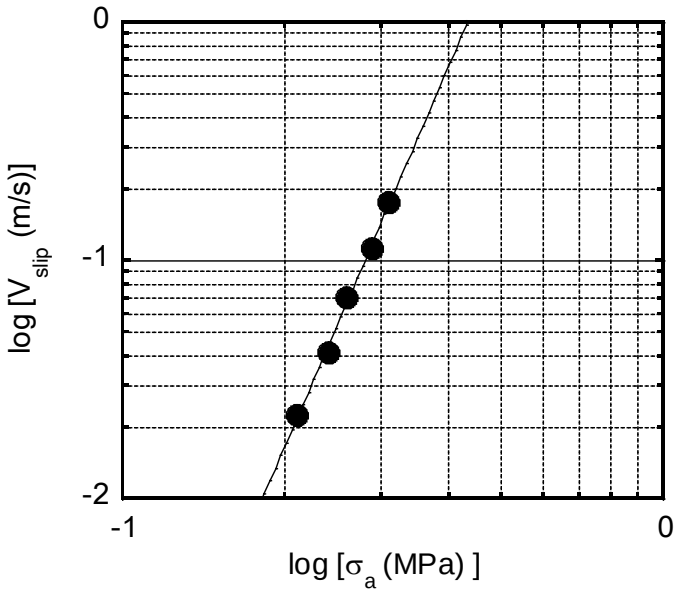

Figure10 Slip velocity as a function of the apparent shear stress on the wall at 300 °C in the super-extrusion region.

4. Conclusion

Flow instability of ETFE at the capillary extrusion is evaluated. It is found that ETFE shows several types of flow instabilities. In relatively low shear rate region, the shark-skin failure appears beyond the critical shear stress 1.9×10^4 Pa, which usually decides the maximum production speed at extrusion. Furthermore, the slip-stick failure occurs at 1.8×10^5 Pa and wavy melt fracture, originated from the flow instability at die entrance, appears over 3.5×10^5 Pa. It is interesting to note that quasi-stable flow region, so-called super-extrusion, is detected between slip-stick and wavy melt fracture regions. Since the surface of the extruded strand is smooth enough without volumetric distortion, ETFE can be processed at a high out-put rate condition by the steady slippage. The slip velocity is characterized by the Mooney method. The critical shear

stress of the slippage on the wall is found to be 1.8×10^5 Pa, which corresponds to the onset stress of the slip-stick failure.

References

[1] F.N. Cogswell, Polymer Melt Rheology, George Godwin, London, 1981.

[2] J.M. Piau, J.F. Agassant, Rheology for Polymer Melt Processing, Elsevier, Amsterdam, 1996.

[3] S.G. Hatzikiriakos, K.B. Migler, Polymer Processing Instabilities, Marcel Dekker, New York, 2005.

[4] R. Koopmans, J.D. Doelder, J. Molenaar, Polymer melt fracture, CRC press, New York, 2010.

[5] M. Meller, A. Luciani, A. Sarioglu, J.E. Manson, Polym. Eng. Sci. 42 (2002) 611-633.

[6] F. Brochard, P.G. De Gennes, Langmuir 8 (1992) 3033–3037.

[7] A. Allal, A. Lavernhea, B. Vergnesb, G. Marin, J. Non-Newtonian Fluid Mech. 134 (2006) 127-136.

[8] A. Allal, B. Vergnesb J. Non-Newtonian Fluid Mech. 146 (2007) 45-50.

[9] M. Yamaguchi, H. Miyata, V. Tan, C.G. Gogos. Polymer 43 (2002) 5249-5255.

[10] E. Rosenbaoum, Rheology and processability of FEP resins for wire coating Ph.D. dissertation, The University of British Columbia, Vancouver, 1998.

[11] X.-Y. Chen and Y.-M. Zhang, J. Appl. Polym. Sci. 125 (2012) 2442-2448.

[12] B. Ameduri, B. Boutevin, Well-Architectured Fluoropolymers: Synthesis, Properties and Applications, Elsevier, Amsterdam, 2004.

[13] J.G. Drobny, Technology of Fluoropolymers, 2nd Ed., CRC Press, Boca Raton, 2009.

[14] S. Kotera, M. Yamaguchi J. Fluorine Chem. 166 (2014) 117-121.

[15] K. Linliu, B. Chu, Polymer 36 (1995) 2265-2269.

[16] L.H. Tung, J. Polym. Sci. 46 (1960) 409-422.

[17] B. Chu, J. Wang, W. Tuminello, J. Appl. Polym. Sci. 498 (1993) 97-101.

[18] G. Ajiroldi, C. Garbugio, M. Ragazzini, J. Appl. Poly. Sci. 14 (1970) 79-88.

[19] A.B. Tobolsky, D. Katz, M. Takahashi, J. Polym. Sci. Part A 1 (1963) 483-489.

[20] D.S. Kalika, M. M. Denn, J. Rheol. 31 (1987) 815-834.

[21] K. Jordes, G.L. Willkes, J. Janzen, D.C. Rohlfing, M.B. Welch, Polymer 41 (2000) 7175-7192.

[22] D. Yan, W.-J. Wang, S. Zhu, Polymer 40 (1999) 1737-1744.

[23] S. Wu, J. Polym. Sci. Polym. Phys. 27 (1989) 723-741.

[24] J.D. Ferry, Viscoelastic Properties of Polymers, 3rd Ed., Wiley, New York, 1980.

[25] N.J. Mills, Nature 219 (1968) 1249-1250.

[26] O. Saito, The Radiation Chemistry of Macromolecules, Academic Press, New York, 1972.

[27] J.P. Tordella, Unstable flow of molten polymers, in: F.R. Eirich (Ed.), Rheology Vol.5, Academic Press, New York, 1969, 57-92.

[28] G.V. Vinogradov, N.I. Insarova, B.B. Boiko, E.K. Borisenkova, Polym. Eng. Sci. 12 (1972) 323-334.